Simple solutions for square and rectangular cofferdam seepage problems

Thushara Asela Madanayaka[1], Nagaratnam Sivakugan, Ph.D., P.E., F. ASCE[2]

[1]PhD Candidate, College of Science and Engineering, James Cook University, Townsville, QLD 4811, Australia. (Corresponding Author), E-mail: thushara.madanayaka@my.jcu.edu.au

[2]Associate Professor, College of Science and Engineering, James Cook University, Townsville, QLD 4811, Australia. E-mail: siva.sivakugan@jcu.edu.au

Abstract:

Cofferdams are widely used temporary structures in the construction sites. Two of the main parameters required in designing a cofferdam are the flow rate and exit hydraulic gradient at the bottom of the excavation. Commonly, these two parameters are evaluated by using the 2D ground water flow models. However, when the flow pattern is three-dimensional, such as flow into the square or rectangular cofferdams, predictions by the 2D models underestimate the flow rate and exit gradients considerably. Therefore, it is necessary to incorporate the 3D flow effect through a correction factor. It is shown that treating a square cofferdam as a circular one of the same width or treating a rectangular cofferdam as 2D double-walled cofferdam significantly underestimates the flow rate. In this study, simple expressions are developed and validated for accurately estimating the flow rate and exit hydraulic gradient values of square and rectangular cofferdams, based on hundreds of finite element simulations in both 2D and 3D. It is suggested that the expressions given in the Canadian Foundation Engineering Manual be improved.

Keywords: Flow rate, Exit hydraulic gradient, Square cofferdam, Rectangular cofferdam

Introduction

Cofferdams are widely used in construction sites as temporary structures to keep excavations safe and dry, reducing the water seepage into the excavations. They are constructed by making enclosures using walls of sheet piles driven into the ground. Within the enclosure, the soil is excavated while water seeps into the excavation. Long-narrow, circular, square and rectangular shapes in plan view are the cofferdam types commonly seen in practice. Constructions of dams, quarry walls and bridge piers are typical examples of the situations where long-narrow type cofferdams are applied (Banerjee 1993). The circular cofferdams are commonly involved with the constructions of sewers, bridge piers and abutment and shaft (Koltuk and Azzam 2016). Some of the significant case histories on the application of circular cofferdams have been reported by Lefas and Georgiannou (2001), Parashar et al. (2007), Underwood and Weber (2011) and Tan and Wang (2015). Square or rectangular cofferdams are encountered with the excavation for building foundations, small bridges or river pier foundations.

Flow rate Q and exit hydraulic gradient i_E are two key parameters in designing the sheet pile cofferdam of any shape. The flow rate is important to determine the required number and capacity of water pumps to keep the excavation area dry, and the exit hydraulic gradient i_E is necessary to estimate excavation base stability against piping failure, which is more likely to happen in non-cohesive soil. Underestimating the flow rate adversely affects the workers safety within the excavation making the excavation base inundate. This is because the dewatering pump capacity is designed based on the estimated flow rate, and when it is lower than actual, employed pumps cannot maintain the excavation base dry. Besides, the effect of underestimating the exit hydraulic gradient is also on to the unsafe side since the actual factor of safety against piping failure is lower than estimated one. Therefore, accurate estimation of

the flow rate and exit hydraulic gradient is a vital factor in designing a cofferdam of any shape. However, the type of analysis required for estimating the flow rate Q and exit hydraulic gradient i_E varies with the cofferdam shape.

When the enclosure shape is the long-narrow, the cofferdam type is termed as double-walled since the length is considerably large compared to its width, and hence, the two long walls are assumed parallel. Therefore, seepage analysis for this case is a 2D problem can be carried out in the Cartesian co-ordinates system, treating the third dimension as infinite. Further, circular cofferdam problems can also be analysed as 2D problem even though the flow pattern into the circular cofferdam is three-dimensional, considering the axisymmetric nature. Therefore, 2D seepage analysis in the cylindrical co-ordinates system (axisymmetric analysis) is the appropriate one for the circular cofferdams. However, when the cofferdam shape is square or rectangular, 3D seepage analysis is the only option since the 2D approximation considering the situation as double-walled cofferdams can jeopardize safety. In the three-dimensional situations, the flow paths in all directions give higher Q and i_E than what is predicted using a 2D analysis, assuming a double-walled cofferdam. This has been discussed by several researchers based on laboratory model tests and case histories (Bauer 1984; Tanaka et al. 2002; Tanaka and Yokoyama 2005; Bouchelghoum and Benmebarek 2011; Koltuk and Iyisan 2013; Tanaka et al. 2013).

All the cofferdam types mentioned above are similar in the cross-sectional elevation to the one shown in Fig. 1a where the seepage flow is taking place under the total head difference of h. L and r are the half-width and radius of the double-walled and circular cofferdams, respectively. B represents the half-length of each side of the square cofferdam and half-width of rectangular cofferdam at the shorter side while l denotes half-length of a rectangular

cofferdam at the longer side. The sheet pile embedded depth, outside the excavation is s, and T is the thickness of the permeable layer. Even though, all the cofferdams are similar in the cross-sectional view, their flow patterns are different, as shown in Fig.1b. The one in top left is for the double-walled case (parallel flow) while the one at top right is for the circular cofferdam. The bottom left in Fig.1b is for the square cofferdam, and the bottom right represents rectangular cofferdam.

The 2D problems in Cartesian plane can be solved using flow nets or numerical methods involving finite element or finite difference methods. In addition, there are approximate solutions derived from the method of fragments (MoF) that can give reasonable estimates of Q and i_E. Griffiths (1984) introduced MoF solutions for the double-walled cofferdams and Madanayaka and Sivakugan (2016) and Madanayaka et al. (2017) discussed these in more detail.

There is very little literature available on the solution methods for three-dimensional problems involving circular, square or rectangular cofferdams. These problems require 3D numerical simulation packages. However, for the circular cofferdams, it is possible to use 2D numerical modelling packages, which can treat the problem as axisymmetric. Neveu (1972) developed design charts to estimate the flow rate for the circular cofferdams using the Green's Theorem, considering them as axisymmetric problems. Moreover, few studies have presented design charts using the 3D numerical simulations for circular cofferdams (Miura et al. 2000; Bouchelghoum and Benmebarek 2011; Koltuk and Azzam 2016). More recently, Madanayaka and Sivakugan (2017) proposed method of fragments (MoF) solutions for estimating the flow rate and exit hydraulic gradient for the circular cofferdams. In addition, Becker and Moore (2006) have presented an approximate method for predicting the flow rate

and exit gradient for the circular and square type cofferdams using corresponding values of double-walled cofferdams of same geometry in the elevation.

However, 3D numerical simulation is still the only accurate option for the rectangular cofferdams, but it requires an expensive 3D simulation package. So, there is a perceived benefit in having a simple approximate method for solving the rectangular cofferdam problems since they are among the commonly used cofferdam types. The object of this paper is to propose expressions for determining Q and i_E of square and rectangular cofferdams. These expressions are developed based on hundreds of simulations using 3D finite element analysis. The solutions are also compared with those provided in the Canadian Foundation Engineering Manual (CFEM) in 2006.

Seepage solution for square cofferdams

Numerical simulation using a 3D computer package is the most accurate solution method for the square cofferdams. However, due to the significant cost and advanced resources requirement in 3D simulations, two alternative approaches are practiced in industry as outlined below.

1. Axisymmetric approximation, considering square cofferdam is equivalent to the corresponding circular one of the same width (i.e., $B = r$) (Tanaka and Yokoyama 2005; Bouchelghoum and Benmebarek 2011).
2. Predict the values using the corresponding values from double-walled cofferdam and apply a correction factor proposed by the Becker and Moore (2006) in the CFEM.

In this study, accuracy of the two methods mentioned above are compared using the flow rate and exit gradient values derived through the 3D finite element program (RS3 2.0) developed

by Rocscience. Here, predictions by the above two methods were compared against the actual flow rate and exit gradient calculated by 3D simulations.

Numerical simulations

The finite element programs RS2 9.0 and RS3 2.0 developed by the Rocscience were used to simulate the 2D cofferdam models (axisymmetric cofferdams and double-walled cofferdams) and 3D square cofferdams, respectively. The numerical model applied for the square cofferdam is shown in Fig.2a while Fig.2b shows the corresponding 2D model used for both circular and double-walled cofferdams. The only difference between the circular and double-walled simulation was the analysis type. Axisymmetric analysis was used for the circular cofferdams simulations while it was plane strain in the double-walled cases. In the square cofferdam analysis, only one of the four quadrants were considered while one-half of the cross sections are analysed for circular and double-walled cofferdams, considering the symmetry. The definitions of the parameters, h, B, L, r, s, and T are similar to those defined in Fig.1a. The excavation depth within the cofferdam is αs where $0 \leq \alpha < 1$. For all the simulations, a homogeneous and isotropic soil model was applied; therefore, the soil permeability was kept constant within the entire model.

Further, it is assumed that the seepage flow into the excavation does not lower the ground water table, outside the excavation for all the cases. This assumption is reasonable when the cofferdam is used in the offshore excavation as shown in Fig. 2. Moreover, this is a conservative assumption when the cofferdam is for the onshore excavations, where the water table is below the ground level, outside the excavation. Fig. 3 shows the initial dewatering condition of the onshore cofferdam. When dewatering the inner excavation is progress, the water table outside the excavation starts to lower and reaches a steady state condition after

some time. The transition time required depends on the soil permeability, depth of the sheet pile penetration below to the water table and the width of the excavation (Kavvadas et al. 1992). Hence, the most critical flow condition is encountered at the initial dewatering condition for the onshore cofferdams, and at which flow rate, exit hydraulic gradient and hydraulic pressure on the sheet pile wall are the highest. Therefore, all the designing parameters (flow rate, factor of safety against hydraulic failure and the strength of sheet pile wall) of onshore cofferdam must be based on the critical flow condition, i.e., the initial condition. Accordingly, numerical solutions of offshore cofferdams are applicable to the onshore cases also; however, it is required to consider embedded depth of the sheet pile s as the distance between water table and tip of the sheet pile (see Fig. 3). Thus, all simulations in this paper were conducted for the offshore cofferdam models (Fig. 2).

In all the simulations, planes/axis of symmetry and impermeable bases were considered as impermeable boundaries. The ground level outside the excavation and excavation base level were treated as constant head boundaries with the total head difference of h. All the simulations were carried out as flow only problems for a completely saturated soil, and a graded mesh with ten-noded tetrahedral elements were used for 3D meshing of square cofferdams while uniform mesh with four-nodded quadrilateral elements were employed for 2D meshing. In addition, a thin layer of material was used to simulate sheet pile wall where its permeability is orders of magnitude lower than the soil material.

Validity of the numerical models

Before studying the seepage beneath cofferdams, 2D and 3D models were calibrated against the result of the extensive experimental study conducted by the Davidenkoff and Franke

(1965) using the electrical analogy model for circular and square cofferdams. The geometries considered for the numerical models validations are shown in Table 01.

Axisymmetric model for circular cofferdam

Flow rate estimation

For the validation, dimensionless flow rate values (q_c/kh) measured by the Davidenkoff and Franke (1965) for the circular cofferdam geometries (shown in Table 01) were compared against the corresponding dimensionless flow rate values (q_c/kh) estimated by the numerical simulations using the RS2 9.0 package. Here, q_c is the flow rate along the meter perimeter length of the circular cofferdam. The comparison results are shown in Fig. 4a.

Exit gradient estimation

Davidenkoff and Franke (1965) defined the dimensionless parameter $\emptyset_s$ which describes the head loss from tip of the sheet pile (point P on Fig. 1a) to the excavation base as a fraction of the total head loss over the cofferdam. Hence,

$$\emptyset_s = \frac{Head\ loss\ from\ pile\ tip to\ the\ excavation\ base}{Total\ head\ loss\ (h)} \quad (1)$$

Then, average exit gradient $i_{E\ Avg.}$ along the sheet pile wall within the excavation can be estimated as:

$$i_{E\ Avg.} = \frac{\emptyset_s h}{Length\ from\ pile\ tip\ to\ excavation\ base} \quad (2)$$

For each numerical model, $\emptyset_s$ value was calculated using the total head value at pile tip (see Eq.1), and relevant average exit gradient i_{EAvg} was evaluated as per the Eq. 2. Again, corresponding average exit gradient $i_{E\ Avg}$ for each model was calculated based on the $\emptyset_s$ values derived experimentally by the Davidenkoff and Franke (1965). For the assessment of

model validity, normalised average exit gradient (i_{EAvg}/h) based on the numerical simulations compared against the predictions by the experimental result as shown in Fig. 4b.

Both comparisons for circular cofferdams show excellent agreement between the experimental results and numerical model results. All the flow rate and exit gradient predictions by the numerical simulations are within the ± 5% to the corresponding experimental results. Therefore, it is verified that the accuracy of the axisymmetric numerical model for analysing the seepage beneath circular cofferdams is adequate. In view of that, numerical model used for the double-walled cofferdam was not validated as a separate model since the same model was used for simulating the double-walled cofferdam because the both analysis are in 2D plane and similar in cross sections (see Fig. 2b). The only difference is the analysis type, which is axisymmetric analysis for the circular cofferdam cases while plane strain analysis is applied for the double-walled simulations.

3D models for square cofferdam

For the validation, dimensionless flow rate (q_s/kh) of the square cofferdam measured by the Davidenkoff and Franke (1965) compared to the corresponding values by the 3D numerical simulations using the RS3 2.0 package. Here, q_s gives flow rate per meter along the perimeter length of the square cofferdam. Fig. 5a shows the comparison of the results. Next, normalised average exit gradient values ($i_{E\ Avg}/h$) calculated based on the numerical simulations and experimental results using similar procedure discussed in axisymmetric model evaluation were compared as shown in Figs. 5b and 5c. Fig. 5b shows the average exit gradient value comparison at the middle of a side of the cofferdam ($i_{EM\ Avg}/h$) while Fig. 5c compared the values at the corner of the cofferdam ($i_{EC\ Avg}/h$). All the comparisons show a good agreement between numerical model predictions and corresponding experimental

results. In flow rate estimations, all the predictions by numerical model deviate less than 10% from the experimental values while all the average exit gradient values (at mid and corner points) are within ± 5%.

In terms of the degree of accuracy of the experimental results, Davidenkoff and Franke (1965) stated that their results can be within the ±5% considering the errors in electrical measuring instruments and the influence of electrolysis and diffusion on the model. Further, they have mentioned that solving the square cofferdam problems using electric analogy is more difficult compared to the circular cofferdam simulations. This is due to the difficulty with the experimental model where the total head value along the cofferdam perimeter could not be accurately modelled in square cofferdams (increasing from mid of the wall to the corner) while this is constant in circular cofferdam models. Therefore, it is expected that the accuracy of experimental result is slightly low with square cofferdams compared to the circular cofferdams. This is observed in our comparison analysis also since the numerical estimations of the flow rate for the circular cofferdams deviate within ±5 % for the circular cofferdam while this is within ±10% for the square cofferdams. Consequently, it can be concluded that both numerical models (axisymmetric and 3D) used in this work are within sufficient accuracy (deviation less than 5% for most of the cases) for simulating the seepage beneath the circular and square cofferdams. In addition, authors did not validate 3D models for the rectangular cases as a separate case since the numerical model used for the rectangular cofferdam analysis was exactly same to the square cofferdam models except changing the length of one side (i.e., 2*l* in Fig 1b).

Sensitivity analysis

Before conducting the extensive parametric study, safe distances from the sheet pile wall to the model's boundary for square (B_e), axisymmetric (r_e) and double-walled (L_e) cases were determined through the sensitivity analysis to ensure that their effects on the seepage result are insignificant. Fig. 6 shows the sensitivity analysis results for the square cofferdams. Here, three geometries were selected (B/T = 0.2, 0.5 and 0.8) when the s/T = 0.5. Noted, for each B/T, three excavation depth values were also considered (α = 0, 0.4 and 0.8) since these combinations give representative results for all cases. Next, the distances from the sheet pile wall to the model's boundary for each geometry were varied by increasing the $(B+B_e)/B$ ratio staring from 2. The safe distance was selected in the way that percentage increment of flow rate q and exit gradient values (i_{EM} and i_{EC}) when the geometry changing from one-step of $(B+B_e)/B$ to the next step is around 1% or lower. Analysis showed that it is negligible the increments of values when $(B+B_e)/B$ ratio changing from 5 to 6 for all the geometries (see Fig. 6a for flow rate, 6b for i_{EM} and 6c for i_{EC}). Therefore, the safe distance from the sheet pile wall to the model's boundary B_e was selected when the ratio $(B+B_e)/B$ equals or greater than 5. Hence, the distance B_e for square cofferdams was selected as equal as or larger than $4B$.

Similar analysis was performed for the axisymmetric and double-walled models and found the safe distances from the sheet pile wall (r_e and L_e). Here also the increments of flow rate and exit gradient values when increasing the model boundary beyond the selected safe distances are within 1%. Then the 2D models (axisymmetric and plane stain analysis) were used for analyzing the seepage beneath the circular and double-walled cofferdams while 3D models were applied for square and rectangular cofferdam simulations. In all the simulations, soil layer thickness T, and head loss h were kept constant, with values of 20 m and 10 m, respectively while treating the soil as homogeneous and isotropic (R = 1) with the

permeability k of 10^{-5} m/s. The soil anisotropy ratio R is defined as $R=\sqrt{k_V/k_H}$, where k_V and k_H are the soil permeability in vertical and horizontal directions, respectively.

Study of square cofferdams

Series of models were studied for the square cofferdams, with three B/T values of 0.2, 0.5 and 0.8 to represent wider range of geometries expected in practice. For each B/T value, three sheet pile embedded depths were analysed for the s/T = 0.2, 0.5 and 0.8 while considering the five excavation depths with α = 0, 0.2, 0.4, 0.6 and 0.8. In each case, flow rate and the two exit hydraulic gradient values adjacent to the sheet pile walls (i_{EC} and i_{EM}) were calculated. i_{EC} is the exit hydraulic gradient at the corner of the square cofferdam where two sheet pile walls meet while i_{EM} gives exit gradient at the mid-point of the sheet pile wall (see Fig.2a). Next, for each square geometry studied, corresponding circular and double-walled cofferdams were analysed (i.e, $L = B$ for the double-walled one and $r = B$ for the circular cofferdam) and the flow rate and exit gradient values were calculated.

Accuracy assessment for the flow rate estimation of square cofferdams

For the assessment, 45 cases, were analysed. Here, flow rate values of square cofferdam q_s (per meter length of the cofferdam perimeter) calculated through the flow rate values derived by 3D numerical simulations and were plotted against the corresponding flow rate values q_c and q_d for the circular and double-walled cofferdams, respectively, in Figures 7a and 7b. Here, q_c and q_d are also the flow rates per meter length of the cofferdam perimeter. For the square cases, cofferdam perimeter equals to the $8B$ while this is $2\pi r$ and $4(B+l)$ for the circular and rectangular cofferdams, respectively. q_c and q_d show strong linear relationships to the q_s.

From Fig.7a,

$$q_s = 1.07q_c \quad (3)$$

The total flow rate Q_s into the square cofferdam can be estimated by multiplying q_s by the perimeter and hence:

$$Q_s = 1.07q_c 8B = 8.56q_c B \quad (4)$$

For equivalent square cofferdam approximated as a circular cofferdam of the same width, the total flow into the excavation Q_s is given by:

$$Q_s = q_c 2\pi B = 6.28q_c B \quad (5)$$

Therefore, from Eqs. 4 and 5, it can be seen that treating a square cofferdam as an equivalent circular cofferdam underestimates the flow rate by 27%.

Similarly, from Figure 7b, Q_s can be estimated via q_d as:

$$Q_s = 0.97q_d 8B = 7.7q_d B \quad (6)$$

From Fig.7, it is clear that, the q_s-q_c relation is stronger than the q_s-q_d relation, with slightly higher coefficient of determination (R^2). The Q_s values computed using Eqs. 4 and 6 are compared in Fig. 8 with the actual values determined from the 3D simulations.

Fig. 8a shows the comparison between actual flow rate and the flow rate predictions using q_c in Eq. 4 while Fig. 8b compares the predictions using q_d in Eq. 6. In Fig. 8a, 30 points out of the 45 (67%) are within the ± 15% while it is 25 (56%) in the Fig 8b. In addition, maximum underestimation of the flow rate is 11% for the Eq. 4 (Fig. 8a) while this is 16% for the Eq. 6 (Fig. 8b). Further, maximum overestimation is by 37% for Eq. 4 with only 8 cases greater than the 30%. In Fig.8b, maximum overestimation was 83% and, with 8 cases exceeding 50%. Therefore, it can be concluded that deriving the flow rates for a square cofferdam based on circular cofferdam (Eq. 4) is slightly better than those derived from the double-walled cofferdam (Eq. 6).

In addition, the expression proposed in the CFEM (2006) for predicting the flow rate into the square cofferdam was compared against the relation found in this study (Eq. 6). The expression in the CFEM (2006) can be presented (considering the half width of the square cofferdam by *B*) as:

$$Q_s = 0.7\left[\frac{kh}{\varphi_1+\varphi_2}\right]8B \tag{7}$$

The term $\left[\frac{\mathrm{kh}}{\varphi_1+\varphi_2}\right]$ provides the flow rate per meter length into the half section of double-walled cofferdam using the method of fragment (MoF) where $\varphi_1$and φ_2 are the form factors of the fragments A and C (see Fig. 9). The parameters, *k* and *h* are the soil permeability and head loss across the cofferdam, respectively. Madanayaka et al. (2017) compared numerical model simulation results for the series of double-walled cofferdam against the MoF solution and found a very good agreement between them. Therefore, the term $\left[\frac{\mathrm{kh}}{\varphi_1+\varphi_2}\right]$ in Eq. 7 can be replaced by the numerical simulation result q_d for the double-walled cofferdams, and hence:

$$Q_s = 0.7q_d8B = 5.6q_dB \tag{8}$$

Comparing Eqs.6 and 8, it is clear that CFEM (2006) predictions are significantly lower than the predictions by the proposed expression (Eq. 6) in this study. To compare the two equations further (to see their deviation from the actual flow rate), predictions by Eqs. 6 and 8 are plotted against the actual total flow rate Q_s , in a same graph (see Fig. 10). Fig. 10 shows that, most predictions by the Eq. 8 are underestimates, i.e., 37/45 (82%) with maximum deviation of 40%. Also, only 12 points remain within the range of ± 15%. Therefore, Eq. 6 predicts the flow rate better compared to the expression proposed in the CFEM (2006). CFEM (2006) uses φ_1 and φ_2 without explicitly saying they are the form factors used in

MoF. These form factors are computed in CFEM from a graph by treating the two fragments similar to fragment C. They are not similar. Fragment C has a width of L, but fragment A extends to infinity (see Fig. 9). This practice leads to overestimation of φ_1 and hence underestimation of the flow rate. Also fragment A form factors are only a function of the s/T, as shown in Griffiths (1984) and Madanayaka and Sivakugan (2016). φ_1 in CFEM can still be estimated using the same chart but based on d_1/T_1 and $T_2/b = 0$.

Therefore, it can be concluded that the flow rate into a square cofferdam is better predicted using q_c computed for a circular cofferdam of the same width by Eq. 4 than q_d computed for a double-walled cofferdam using Eq. 6 or 8. The q_c for the circular cofferdam can be determined through the 2D simulation as the axisymmetric problem or more easily, via the method of fragment (MoF) solution proposed by Madanayaka and Sivakugan (2017) for axisymmetric cofferdams. However, current industry practice, (i.e., replacing the square cofferdam by an equivalent circular one) is discouraged since flow into a circular cofferdam is about 27% less than the flow into a square cofferdam of the same width (see Eq. 5).

Accuracy assessment for exit gradient estimation of square cofferdams

For the assessment, exit gradient values of the square cofferdam at the mid (i_{EM}) and corner (i_{EC}) points derived by 3D numerical simulation were compared with the corresponding exit gradient i_E values for the circular and double-walled cofferdams (see Fig.11). Circular and double-walled exit gradient values also show strong linear relationship with both i_{EM} and i_{EC}. Fig. 11a shows the relation based on the exit gradient values of circular cofferdams where the left one is for the i_{EM} and right one is for the i_{EC}. The corresponding results based on the exit gradient values of double-walled cofferdam are shown in the Fig. 11b.

From Fig. 11a,

$$i_{EM} = 0.9 i_E \quad (9)$$

$$i_{EC} = 1.24 i_E \quad (10)$$

From Fig. 11b,

$$i_{EM} = 1.26 i_E \quad (11)$$

$$i_{EC} = 1.75 i_E \quad (12)$$

Next a detailed validation was carried out to assess the accuracy of Eqs. 9, 10, 11 and 12, comparing the predictions by above equations to the actual values obtained by 3D simulation for the square cofferdams (see Fig. 12). Fig. 12a shows the comparisons based on the circular cofferdams (Eqs. 9 and 10) while Fig. 12b shows the comparison based on the double-walled cofferdams (Eqs. 11 and 12). For the i_{EM} estimations, prediction by circular exit gradients values (Fig. 12a left) is more accurate than the double-walled one (Fig. 12b left). In Fig. 12a left, all the predictions are within ± 10% while only 27out of 45 predictions by Eq.11 (Fig. 12b left) are within ± 10%. In addition, 14 predictions by Eq.11 are on the unsafe side with the deviation exceeding 10%, and the maximum deviation being 25%. Therefore, Eq. 9 is better than Eq. 11 for estimating i_{EM}.

In the i_{EC} estimations, most of the predictions by both Eqs. 10 and 12 are on the conservative side, i.e., 36/45 and 35/45 predictions from Eq. 10 and Eq. 12, respectively, overestimating the exit gradient. However, most of the predictions (30/45) by the Eq.12 are within the ± 15% while it is only (20/45) for the Eq.10. Also, maximum deviation to the unsafe side is 22% by the Eq. 10, but this is within 15% for Eq. 12 predictions. In contrast, maximum overestimate prediction by the Eq. 10 is 28% while it is 37% with the Eq. 12. Therefore, between the two

methods (Eqs 10 and 12), one is no better than the other. Also, in Figs 11a and 11b or from the Eqs. 9, 10, 11, and 12, it is observed that i_{EC} and i_{EM} are related as:

$$\frac{i_{EC}}{i_{EM}} = 1.38 \tag{13}$$

This relation is useful since one exit gradient can be determined from the other for square cofferdams.

In conclusion, Eq. 9 is more accurate for estimating the exit gradient i_{EM} at the mid-section of the square cofferdam, and numerical simulation or method of fragment (MoF) solutions proposed by Madanayaka and Sivakugan (2017) can be used for finding the corresponding exit gradient value of circular cofferdam. In predicting the i_{EC} both double-walled based or circular based relationships (Eqs.10 or 12) can be used, depending on which of the 2D exit gradient values is available. For both cases, 2D numerical simulation and MoF solutions provide the necessary value. CFEM (2006) provides Eqs. 14 and 15 for determining i_{EM} and i_{EC}, which are in very good agreement with Eqs. 11 and 12. However, the i_E values in these two equations are the average values of the hydraulic gradients within the excavation at the mid-point and corner.

$$i_{EM} = 1.3 i_E \tag{14}$$

$$i_{EC} = 1.7 i_E \tag{15}$$

Seepage solution for rectangular cofferdams

As discussed previously, the only accurate solution method available for the rectangular cofferdams is the 3D numerical simulation. However, due to the cost and advanced resource requirement for 3D simulation, these problems are solved as 2D problems in Cartesian coordinate system (i.e., as double-walled cofferdams). Nevertheless, this approximation is

unsafe especially when the cofferdam length is not considerably larger than its width since the actual flow into the cofferdam is in three-dimensional in these situations. This can significantly underestimate the exit gradient and the flow rate. Therefore, a thorough analysis was performed in this section to identify the safe length to width ratio for the rectangular cofferdam at which 2D approximation is reasonable (neglecting the effects of two shorter sides) for estimating the flow rate and exit hydraulic gradient values.

Numerical simulations of rectangular cofferdams

Fig. 13 shows the numerical model used for rectangular cofferdam analysis using the 3D finite element program (RS3 2.0) developed by Rocscience. Here also, only a quadrant was analysed, taking the advantage of symmetry. The boundary conditions and the parameters h, s, αs, T and R are defined in the same way discussed for the square cofferdam modelling (see Fig.2a left). Here B is the half-width of the shorter side of the cofferdam while l represents the half-length of the longer side. Therefore, the ratio l/B equals the length/width ratio of cofferdam. All the runs were analyzed as flow only problems, and a graded mesh was applied with ten-noded tetrahedral elements for each simulation. The distances from the sheet pile wall to the model's boundaries (B_e for the shorter side and l_e for the longer side) were selected through the sensitivity analysis in a similar way discussed for the square cofferdam solutions, i.e., further increasing of B_e and l_e beyond the selected values increase the flow rate and exit gradient values only by 1% or lower. In all the simulations, values of T, and h were kept constant, with 20 m and 10 m, respectively. The soil was treated as isotropic (R = 1) with permeability of 10^{-5} m/s.

For the analysis, seven l/B ratios were considered as 1, 1.5, 2, 3, 5, 10 and 20, assuming that the geometries where l/B ratio greater than 20 are rarely seen. For each l/B ratio, 45

geometries were analysed, considering three *B/T* values (0.2, 0.5 and 0.8), three *s/T* values (0.2, 0.5 and 0.8) and five excavation depths αs (for α 0, 0.2,0.4,0.6 and 0.8), similar to the way that the square cofferdams were analysed. In each case, flow rate and the three exit hydraulic gradient values adjacent to the sheet pile walls (i_{EC}, i_{ES} and i_{EL}) were calculated. i_{EC} is the exit hydraulic gradient at the corner of the rectangular cofferdam while i_{ES} and i_{EL} give exit gradients at the mid-points of the shorter side and longer side, respectively (see Fig. 13). Next, for each rectangular geometry, flow rate (per meter length of perimeter) and exit gradient of the corresponding double-walled cofferdam (see Fig. 2b) were calculated.

Accuracy assessment for flow rate estimation of rectangular cofferdams

For the assessment, 315 geometries were considered with 45 for each of the seven *l*/*B* ratios. Then calculated flow rate for the rectangular cofferdams using the 3D simulation was divided by relevant *l* value (neglecting the flow across the shorter side) to find the flow rate per meter perimeter length q_r for each model, considering the double-walled approximation. Then, for each the *l*/*B* ratio, q_r values were plotted against the corresponding flow rate of the double-walled cofferdams q_d, in separate graphs. The graph for *l/B* = 3.0 is shown in Fig. 14. It shows strong linear relationship between q_r and q_d of the form of $q_r = aq_d$. Therefore, for *l*/*B* = 3, the flow rate determined from a double-walled cofferdam has to be multiplied by 1.48. The multipliers for other *l*/*B* values are given in Table 2. The variation of *a* against *l*/*B* is shown in Fig 15 and the relation of *a* to the *l/B* can be defined as:

$$a = 1.81(l/B)^{-0.14} \quad (16)$$

Accordingly, total flow rate into the rectangular cofferdam Q_r when $0 < l/B \leq 20$ can be estimated as:

$$Q_r = aq_d 4l = 4aq_d l \quad (17)$$

Also, results in the Table 2 show that even for *l/B* as high as 20, assuming *l/B* as infinite tends to underestimate the flow rate by about 20%, requiring a multiplication factor (a) of 1.25. Here, derived a value is the average value for *l/B* =20 covering a wider range of geometries, i.e., three *B/T* values (0.2, 0.5 and 0.8), three *s/T* values (0.2, 0.5 and 0.8) and five excavation depths αs (for α 0, 0.2,0.4,0.6 and 0.8). Thus, the safe limit for *l/B* ratio at which 2D approximation is reasonable (can neglect the effects of shorter sides), is a function of *B/T*, *s/T* and α, i.e., it depends on the cofferdam geometry, and hence, the concentration of flow into the cofferdam. For instance, geometries where the flow concentrations are the highest (*B/T* = 0.2 and *s/T* = 0.8), the effects of the shorter sides are negligible even for *l/B* = 10 although it is required to multiply 2D flow by 1.25 for *l/B* = 20 on average. Conversely, geometries where the concentrations are the lowest (*B/T* =0.8 and *s/T* = 0.2) require considering the effects of the shorter sides to obtain the actual flow rate even for *l/B* = 20. Therefore, it is not possible to define a reasonable safe limit for the range of *l/B* ratios 1 to 20 considered in this study. As noted before, it is uncommon to see a rectangular cofferdams with *l/B* ratio greater than 20; however, authors suggest using a = 1.19 predicted by Eq. 16 at *l/B* = 20 for any geometries having a larger *l/B* ratio than 20, since these flow rate predictions are on to the conservative side.

The proposed solution method was validated at *l/B* = 3 against the 45 cases, covering the wider geometry range through the steps mentioned below.

1. Estimated the a value at *l/B* =3 from Eq. 16, and it was 1.55.
2. Predicted the total flow rate Q_r from the Eq. 17 and compared the predictions against the actual flow rate estimated by the 3D simulation for all 45 cases. The comparison result is shown in the Fig. 16.

In this validation process, predictions for most of the geometries (28/45) are within ±15% while any underestimation of flow rate is less than 5%. Also, for the 9 cases, where the flowrate is overestimated by 25% or more, the geometries correspond to cases having very little significance in practice where B/T = 0.2 and s/T values equal to 0.5 and 0.8. Overall, proposed Eq. 17 provides reasonable estimates of flow rate, and the few predictions where deviations are large are on the conservative side.

Accuracy assessment for exit gradient estimation of rectangular cofferdams

The 45 geometries above were also considered for six other l/B ratios in Table 2, making a total of 315 geometries. For each geometry, three exit gradient values mentioned previously (i_{EC}, i_{ES} and i_{EL}) were determined using the 3D simulation. Next, for each l/B ratio, these three exit gradient values were plotted in three separate graphs against the exit gradient values of corresponding double-walled cofferdams. The graph for i_{EC} at l/B = 3 is shown in Fig. 17, and here, i_{EC} relates strongly to the corresponding exit gradient values of the double-walled cofferdam in the form of $i_{EC} = bi_E$. All three exit gradient values (i_{EC}, i_{ES} and i_{EL}) for each case of l/B showed similarly strong relation to the exit gradient values of the double-walled cofferdam, and the summary of the analysis is given in Table 03.

The results show that the highest exit gradient values are reported for the corner (i_{EC}) where the seepage forces concentrate more strongly compared to the mid sections of the two sides. Also, second largest exit gradient is reported for i_{ES} i.e., at the mid-point of the shorter side while i_{EL} is the lowest. This is due to higher concentration of streamlines at the shorter side compared to the longer side. For $l/B \geq 3$, b remains constant for all three locations, implying that the i_{EC}, i_{ES} and i_{EL} values remain constants too. Also, for the i_{EC} and i_{ES} estimations, the two critical locations, there is only a slight reduction in b value when l/B changes from 1 to 3.

Therefore, even for l/B values as high as 20, the two critical exit gradients i_{EC} and i_{ES} are significantly higher than what is derived from a 2-dimensional approximation, neglecting the effects of shorter sides. Then, for i_{EC} and i_{ES} estimates, b can be conservatively taken as 1.75 and 1.26, respectively, for all l/B values. Accordingly, following equations are proposed for i_{EC} and i_{ES} for all rectangular cofferdams:

$$i_{EC} = 1.75 i_E \tag{18}$$

$$i_{ES} = 1.26 i_E \tag{19}$$

However, the change of b for i_{EL} estimation is considerable compared to the i_{EC} and i_{ES} estimations. Then, a graph was plotted for estimating the b value for the $0 < l/B \leq 3$ as shown in Fig. 18. The relation of b to the l/B is given as:

$$b = 1.25(l/B)^{-0.16} \tag{20}$$

Accordingly, exit gradient i_{EL} can be estimated when $0 < l/B \leq 3$ as:

$$i_{EL} = b i_E \tag{21}$$

When the l/B ratio greater than 3, it is suggested to conservatively use same b value when l/B is at 3. Also, at $l/B = 3$, $b \approx 1$ and hence, a rectangular cofferdam can be analysed as double-walled one, but only for estimating the i_{EL} for $l/B \geq 3$.

The proposed solutions for the exit gradient estimates [Eqs. 18, 19, and 21] were also validated for the 45 geometries at $l/B = 3$. Here, i_{EC}, i_{ES} and i_{EL} were estimated using the Eqs. 18, 19 and 21, respectively and compared against the actual exit gradient values estimated by 3D simulations. Fig. 19 shows the validation results. In the i_{EC} estimation, 29 cases predicted by the proposed Eq. 18 are within ±15% while maximum underestimation is limited to 7% (Fig. 19a). Also 12 cases overestimated i_{EC} by more than 25%, but most of them are for the

geometries with no significance in practical applications, i.e., B/T = 0.2. For the i_{ES} estimations, 43/45 predictions are within ±15% (see Fig. 19b) while all the prediction for i_{EL} estimations (by Eq. 21) are within ±10% (Fig. 19c). Therefore, it is concluded that proposed Eqs. 18, 19 and 21 predict exit gradient values for the rectangular cofferdams in good level of accuracy, and the few cases where the deviations are significant are always on the safe side.

Effect of seepage on active and passive earth pressure

As discussed in the introduction section, hydraulic failure (piping or heaving) of the excavation base is the mostly serious stability problem asscociated to the seepage flow in cofferdams. However, this is not the only way that seepage flow can make a cofferdam fail. The presene of seepage flow into the excavation increases active earth presure and reduces passive presure; therefore, the effect of seepage is on the unsafe side in terms of structural stability (Kaiser and Hewitt 1982; Soubra et al. 1999; Benmebarek et al. 2006). So, an apprximate rule is applied in practice using the traditional active and passive earth presure coefficient along with the effective soil unit weight γ' for the soil below the water table instead of considering the submerged unit weight γ_{sub} (Craig 2004; Benmebarek et al. 2006). Fig. 20 describes the application of this approximate rule for the double-walled cofferdam case. When the flow direction is downward, γ' equals to $\gamma_{sub}+i\ \gamma_w$ while it is $\gamma_{sub}- i\ \gamma_w$ for the upward flow condition which occurs within the excavation. Here i is the avarage hydrulic gradient along the sheet pile wall assuming uniform dissipation of the total head and is given by $h/[s(2-\alpha)]$. γ_w is the unit weight of the water. Accordingly, effective horizontal stress σ'_{ha} at a point (x distance from the water table) along the sheet pile in the active side is given as:

$$\sigma'_{ha} = K_a(\gamma_m z + \gamma' x) - 2c'\sqrt{K_a} \quad (22)$$

where, K_a is the active earth pressure coefficient, γ_m is the bulk unit weight of the soil above the water table and c' is the effective stress cohesion. For cohesionless soils, $c' = 0$. In the active side, where the flow is downward, $\gamma' = \gamma_{sub} + i\,\gamma_w$. Also effective horizontal stress at the point which is at a depth of y below the water table along the sheet pile in the passive side σ'_{hp} can be defined as:

$$\sigma'_{hp} = K_p \gamma' y + 2c'\sqrt{K_p} \tag{23}$$

Here, K_p is the passive earth pressure coefficient and γ' equals to $\gamma_{sub} - i\,\gamma_w$ since the seepage is in the upward direction of the passive side.

However, average hydraulic gradient in the active side i_a (downward flow) is low compared to the average hydraulic gradient in the passive side i_p due to the resistance to the flow is more in the passive side (upward direction into the excavation) than to the active side. Consequently, assuming a constant average hydraulic gradient i tends to overestimate the both effective active and passive earth pressure components (see the Eqs. 22 and 23). Even though overprediction of active component onto the safe side, it is unsafe to overpredict the passive earth pressure component. Also, net effect of both these predictions are on to the unsafe side in most of the cases since the passive earth pressure coefficient K_p is an order of magnitude larger than the active earth pressure coefficient K_a. Therefore, in this paper, it is suggested to apply method of fragments solutions for finding a more accurate average hydraulic gradient values in the active side i_a and passive side i_p. Accordingly, for the double-walled cofferdam problems, i_a and i_p can be defined as:

$$i_a = \frac{h\varphi_1}{s(\varphi_1+\varphi_2)} \tag{24}$$

$$i_p = \frac{h\varphi_2}{s(\varphi_1+\varphi_2)(1-\alpha)} \tag{25}$$

Here, φ_1 and φ_2 are the form factors of flow fragments in double-walled cofferdams (see Fig. 9). Then more accurate prediction to the effective active (σ'_{ha}) and passive (σ'_{hp}) earth pressure components can be defined as;

$$\sigma'_{ha} = K_a[\gamma_b z + (\gamma_{sub} + i_a\gamma_w)x] - 2c'\sqrt{K_a} \quad (26)$$

$$\sigma'_{hp} = K_p\left[\left(\gamma_{sub} - i_p\gamma_w\right)y\right] + 2c'\sqrt{K_p} \quad (27)$$

Further, i_a and i_p values given by Eq. 24 and 25 can be used for estimating the pore pressure values in both active and passive side of the sheet pile wall. The form factor values for the double-walled cofferdams problems can be obtained through the Griffiths (1984) or Madanayaka and Sivakugan (2016). Similarly, for the circular cofferdam problems, more accurate effective earth pressure values can be obtained using the same Eqs. 24 to 27. The only difference being in the form factor values applicable to the Eqs. 24 and 25, which are the axisymmetric form factor values given by Madanayaka and Sivakugan (2017). Also, axisymmetric form factor values can be used for estimating the approximate earth pressure values at the mid-section of the side of square cofferdams since the total head distribution of both cases are closely related. In the same way, double-walled form factor values are more suitable for the estimating the earth pressure values of mid-section at the longer side of rectangular cofferdams.

Summary and conclusions

Simple solutions for estimating the flow rates and exit hydraulic gradients of square and rectangular cofferdams are presented. Both square and rectangular cases were studied separately. The proposed expressions for flow rate estimations are of the form

$$Q_{3D} = aq_{2D}C \quad (28)$$

where Q_{3D} is the total flow rate into the square or rectangular cofferdam, a is a constant, and C is the perimeter length of the square or rectangular cofferdam. q_{2D} is the flow rate per meter length along the perimeter of the circular or double-walled cofferdam. When estimating the flow rate Q_{3D} for a square cofferdam, it is suggested to use q_{2D} from the circular cofferdam, with a = 1.07 (see Eq. 3). For a rectangular cofferdam, q_{2D} values should be determined from a double-walled cofferdam where a varies between 1.19 and 1.81 depending on l/B (see Eq. 16). Also, it is not safe to consider a rectangular cofferdam as equivalent to the double-walled one even with l/B ratio as high as 20.

In both square and rectangular cofferdams, it is shown that the exit hydraulic gradient is the maximum at the corner. Expressions for the exit hydraulic gradient at the corner and mid-points of the two sides within the excavation are proposed (in rectangular cofferdams, one for short side and one for the long side). All three exit gradients are of the form

$$i_{3D} = b i_{2D} \tag{29}$$

where i_{3D} is the exit hydraulic gradient for the square or rectangular cofferdam, b is a constant, and i_{2D} is the exit gradient of the circular cofferdam for the square cases, and the double-walled cofferdams for the rectangular cases. In square cofferdams, b = 1.24 for the corner and b = 0.90 for the mid-point of any side. In rectangular cofferdams, b = 1.75 for the corner and 1.26 for the mid-point of the short side, and these are independent of the l/B ratio, and hence there is no maximum value for l/B beyond which the problem can be assumed as two-dimensional. For the mid-point of the long side in rectangular cofferdams, b varies between 1.05 and 1.25 depending on l/B (see Eq. 20). However, when the $l/B \geq 3$, a rectangular cofferdam can be considered as a double-walled one, but only for estimating the exit gradient value at the mid-point of the long side.

The proposed expressions, validated using series of finite element simulations, are very valuable for accurately estimating the flow rate and exit gradient values when the flow pattern is in three-dimensional as in square or rectangular cofferdams. Also, more accurate solution methods for estimating the lateral earth pressures when there is seepage is presented.

The solutions proposed in this paper are applicable for the situation where the soil medium is isotropic and homogeneous, i.e., uniform soil thickness along the depth. However, when the soil medium is anisotropic and homogeneous, proposed solutions are still applicable with a reasonable accuracy since the MoF provides the facility to incorporate anisotropic condition in determining the form factors for both double-walled and circular cofferdam cases. For that, it requires to calculate relevant 2D solutions using the MoF first, and then, proposed equations for the square or rectangular cofferdams can be used for finding the appropriate 3D solutions. The solutions proposed herein can be very useful as a design tool in providing realistic first estimates of the flow rate and exit hydraulic gradients, especially in preliminary assessments and for carrying out parametric studies, before going for a detailed analysis.

References

Banerjee, S. 1993. Design Charts for double walled cofferdams. Journal of Geotechnical Engineering ASCE **119**(2): 214-222.

Bauer, G. 1984. Dewatering, hydraulic failure and subsequent analysis of a sheeted excavation. *In* Proc. of Int. Conf. on Case Histories in Geotechnical Eng. pp. 1415-1421.

Becker, D. E., and Moore, I. D. (eds.) 2006. Canadian foundation engineering manual, 4th Ed., Canadian Geotechnical Society, Richmond, BC, Canada.

Benmebarek, N., Benmebarek, S., Kastner, R., and Soubra, A.-H. 2006. Passive and active earth pressures in the presence of groundwater flow. Geotechnique **56**(3): 149-158.

Bouchelghoum, F., and Benmebarek, N. 2011. Critical hydraulic head loss assessment for a circular sheet pile wall under axisymmetric seepage conditions. Studia Geotechnica et Mechanica **33(4)**(4): 3-23.

Craig, R.F. 2004. Craig's soil mechanics. 7th ed, London.

Davidenkoff, R., and Franke, O.L. 1965. Untersuchung der räumlichen Sickerströmung in eine umspundete Baugrube in offenen Gewässern. Tidewellenberechnung nach dem Universalprogramm der BAW(22): 65-75.

Griffiths, D.V. 1984. Rationalized charts for the method of fragments applied to confined seepage. Geotechnique **34**(2): 229-238.

Kaiser, P., and Hewitt, K. 1982. The effect of groundwater flow on the stability and design of retained excavations. Can. Geotech. J. **19**(2): 139-153.

Kavvadas, M., Giolas, A., and Papacharalambous, G. 1992. Drainage of supported excavations. Geotechnical & Geological Engineering **10**(2): 141-157.

Koltuk, S., and Azzam, R. 2016. Design Charts for Circular-Shaped Sheeted Excavation Pits against Seepage Failure by Heave. Periodica Polytechnica Civil Engineering **60**(3): 421-426.

Koltuk, S., and Iyisan, R. 2013. Numerical analysis of groundwater flow through a rectangular cofferdam. Electronic Journal of Geotechnical Engineering (EJGE) **18**.

Lefas, I., and Georgiannou, V. 2001. Analysis of a cofferdam support and design implications. Computers & Structures **79**(26): 2461-2469.

Madanayaka, T., Sivakugan, N., and Ameratunga, J. 2017. Validity of the method of fragments for seepage analysis in double-wall cofferdams. *In* Proc., 19th International Conference on Soil Mechanics and Geotechnical Engineering,, Seoul. pp. 1047-1051.

Madanayaka, T.A., and Sivakugan, N. 2016. Approximate equations for the method of fragment. Int. J. Geotech. Eng. **10**(3): 297-303.

Madanayaka, T.A., and Sivakugan, N. 2017. Adaptation of Method of Fragments to Axisymmetric Cofferdam Seepage Problem. Int. J. Geomech.(9): 10.1061/(ASCE)GM.1943-5622.0000955. doi: 10.1061/(ASCE)GM.1943-5622.0000955.

Miura, K., Supachawarote, C., and Ikeda, K. 2000. Estimation of 3D seepage force inside cofferdam regarding boiling type of failure. *In* Geoteh–Year 2000, Bangkok, Thailand. pp. 371-380.

Neveu, G. 1972. Axisymmetrical seepage flow throgh a circular sheet pile cofferdam. *In* Civil Engineering & applied mechanics. McGill Univ., Montreal.

Parashar, S., Mitchell, R., Hee, M.W., Sanmugnathan, D., and Nicholson, G. 2007. Performance monitoring of deep shafts at Changi WRP project, Singapore. *In* 7th FMGM 2007: Field Measurements in Geomechanics. pp. 1-12.

Soubra, A.-H., Kastner, R., and Benmansour, A. 1999. Passive earth pressures in the presence of hydraulic gradients. Géotechnique, The Institution of Civil Engineers **49**(3): 319-330.

Tan, Y., and Wang, D. 2015. Structural behaviors of large underground earth-retaining systems in Shanghai. I: Unpropped circular diaphragm wall. Journal of Performance of Constructed Facilities **29**(2): 04014058.

Tanaka, T., Hori, H., and Inoue, K. 2002. Boiling occurred within a braced cofferdam due to two dimensionally concentrated seepage flow. *In* 3rd international symposium, geotechnical aspects of underground construction in soft ground. pp. 33-38.

Tanaka, T., Kusumi, S., and Inoue, K. 2013. Effects of plane shapes of a cofferdam on 3D seepage failure stability and axisymmetric approximation. *In* Proceedings of the 18th International Conference on Soil Mechanics and Geotechnical Engineering. pp. 02-05.

Tanaka, T., and Yokoyama, T. 2005. Effects of jet grouting under sheet piles on seepage failure stability of soil. *In* Procs. of the 5th International Symposium on Geotechnical Aspects of Underground Construction in Soft Ground (IS-Amsterdam 2005). pp. 923-929.

Underwood, C.A., and Weber, B.A. 2011. The Use of Reliability Analyses in the Design of Deep Excavations in Soft Clay, Fargo, North Dakota, USA. *In* Geo-Frontiers 2011: Advances in Geotechnical Engineering. pp. 3321-3331.

Figure captions

Fig. 1. (a) Elevation and (b) plan views of a cofferdam under four possible flow patterns

Fig. 2. Numerical models; (a) 3D model for square cofferdams (b) 2D model for double-walled and circular cofferdams

Fig. 3. 2D model of double-walled and circular cofferdams for the onshore excavations

Fig. 4. Circular cofferdam model validation (a) flow rate; (b) exit gradient

Fig. 5. Square cofferdam model validation (a) flow rate; (b) exit gradient at middle of a side (c) exit gradient at corner

Fig. 6. Sensitivity analysis results for square cofferdams (a) flow rate; (b) exit gradient at mid-section (c) exit gradient at corner

Fig. 7. Relationship between 2D flow rates to the 3D flow rate into square cofferdam; (a) axisymmetric flow (b) Cartesian flow

Fig. 8. Comparison of the flow rate predictions for square cofferdams using 2D flow patterns; (a) axisymmetric flow (b) Cartesian flow

Fig. 9. Method of fragments (MoF) in double-walled cofferdam

Fig. 10. Deviation of the flow rate predictions by Eq. 6 and Eq. 8 from the actual flow rate

Fig. 11. Relationships between 2D exit gradient i_E values and the actual exit gradient values of square cofferdams i_{EM} and i_{EC} : (a) axisymmetric flow (b) Cartesian flow

Fig. 12. Comparison of the exit gradient predictions using 2D flow patterns (a) axisymmetric flow (b) Cartesian flow

Fig. 13. Numerical model for rectangular cofferdam

Fig. 14. Relationship between double-walled flow rate to the 3D flow rate into rectangular cofferdam

Table 1. Cofferdam geometries used for numerical models validations

Circular cofferdams			Square cofferdams		
r/T	*s/T*	α	*B/T*	*s/T*	α
0.34	0.13	0.00	0.34	0.12	0.06
	0.13	0.50		0.11	0.45
	0.25	0.00		0.22	0.03
	0.25	0.50		0.21	0.47
	0.50	0.00		0.42	0.02
	0.50	0.50		0.41	0.49
	0.80	0.00			
	0.80	0.50			
0.67	0.11	0.00	0.67	0.14	0.14
	0.11	0.51		0.13	0.46
	0.26	0.00		0.24	0.06
	0.26	0.50		0.22	0.45
	0.51	0.00		0.44	0.03
	0.50	0.50		0.43	0.47
	0.80	0.00		0.84	0.02
	0.80	0.50		0.83	0.49
1.34	0.21	0.05	1.34	0.28	0.15
	0.21	0.52		0.26	0.47
	0.51	0.02		0.47	0.07
	0.51	0.51		0.45	0.46
	0.80	0.00		0.87	0.04
	0.80	0.50		0.85	0.48
3.27	0.51	0.05	3.36	0.70	0.15
	0.51	0.52		0.66	0.47
	0.76	0.03		0.94	0.10
	0.76	0.52		0.88	0.47

Table 2. Summary of the flow rate analysis

l/B	a	R^2
1	1.94	0.92
1.5	1.71	0.94
2	1.61	0.95
3	1.48	0.96
5	1.37	0.97
10	1.29	0.97
20	1.25	0.97

Table 3. Summary of the exit gradient estimation relations

l/B	i_{EL}		i_{ES}		i_{EC}	
	b	R^2	b	R^2	b	R^2
1	1.26	0.97	1.26	0.97	1.75	0.97
1.5	1.15	0.98	1.22	0.98	1.69	0.97
2	1.10	0.99	1.21	0.98	1.68	0.97
3	1.05	0.99	1.19	0.98	1.67	0.97
5	1.02	0.99	1.19	0.98	1.66	0.97
10	1.00	0.99	1.19	0.98	1.66	0.97
20	1.00	0.99	1.19	0.98	1.66	0.97

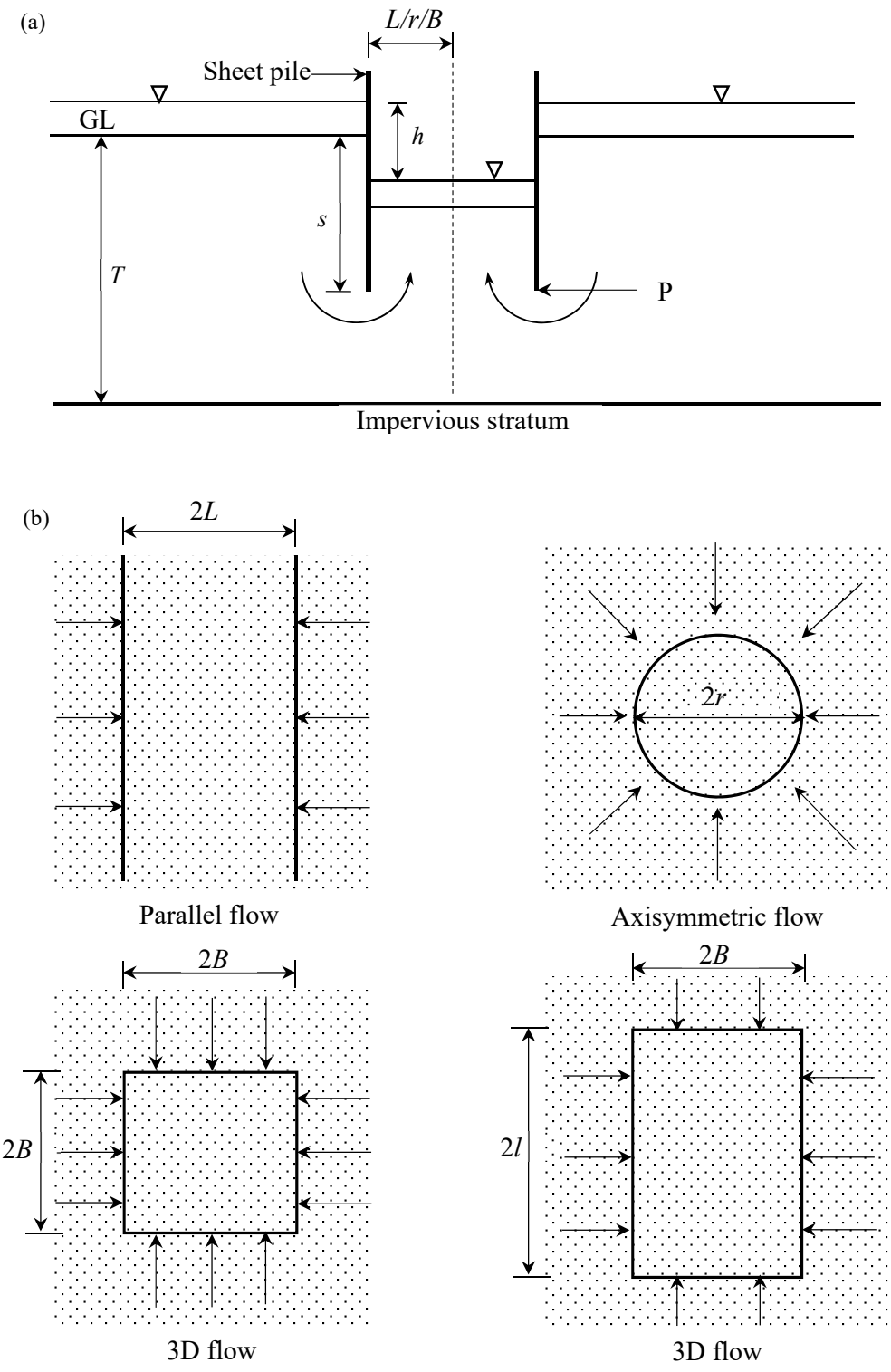

Fig. 1. (a) Elevation and (b) plan views of a cofferdam under four possible flow patterns

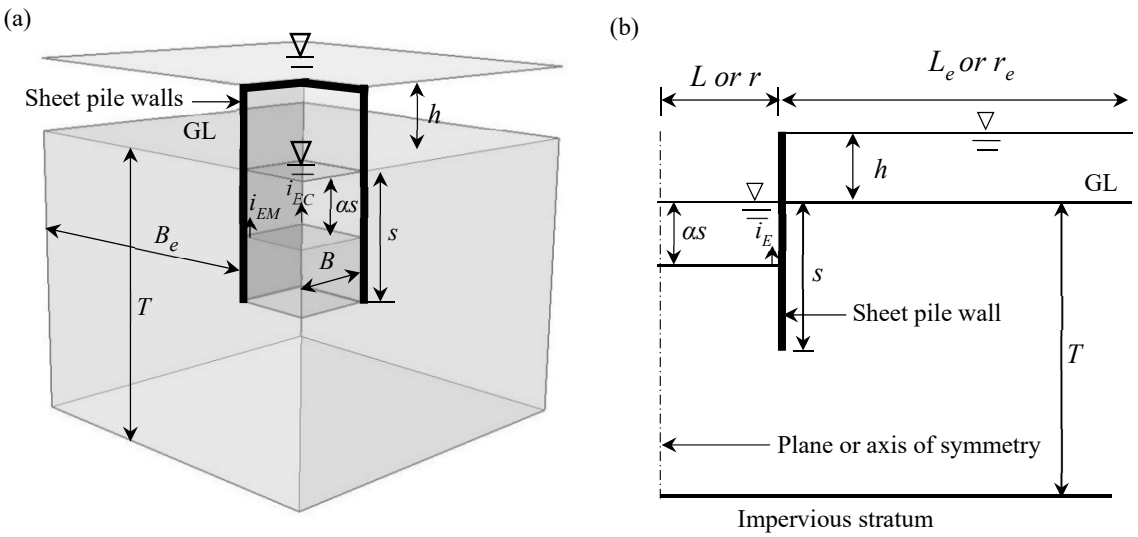

Fig. 2. Numerical models; (a) 3D model for square cofferdams (b) 2D model for double-walled and circular cofferdams

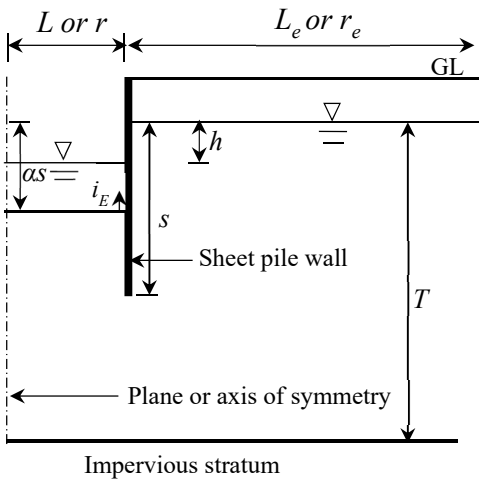

Fig. 3. 2D model of double-walled and circular cofferdams for the onshore excavations

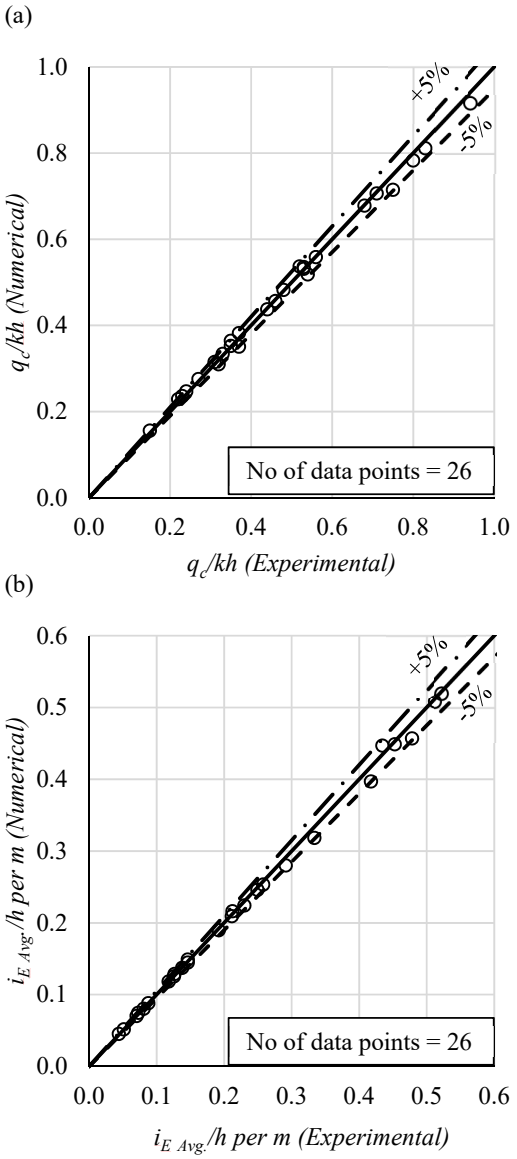

Fig. 4. Circular cofferdam model validation (a) flow rate; (b) exit gradient

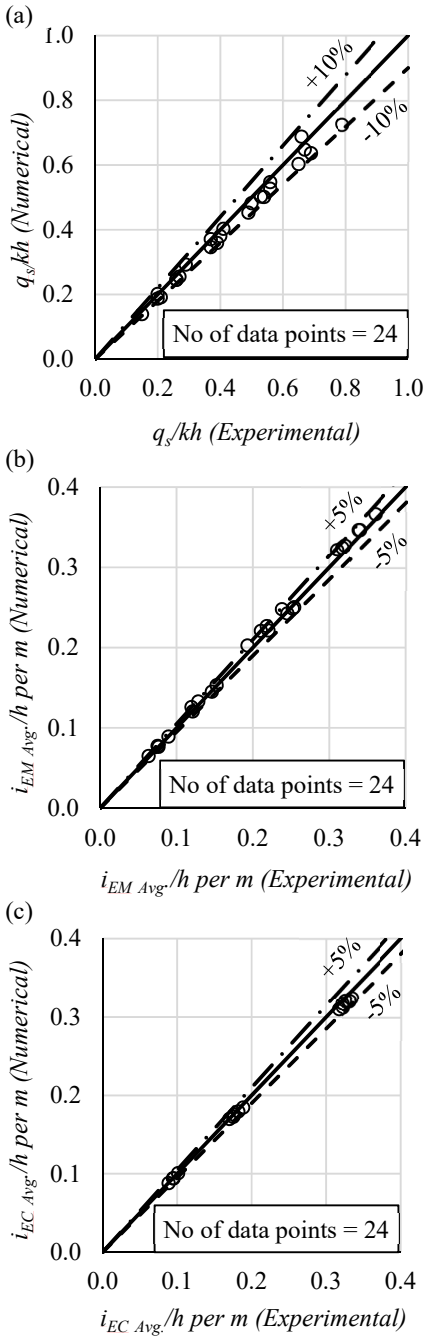

Fig. 5. Square cofferdam model validation (a) flow rate; (b) exit gradient at middle of a side

(c) exit gradient at corner

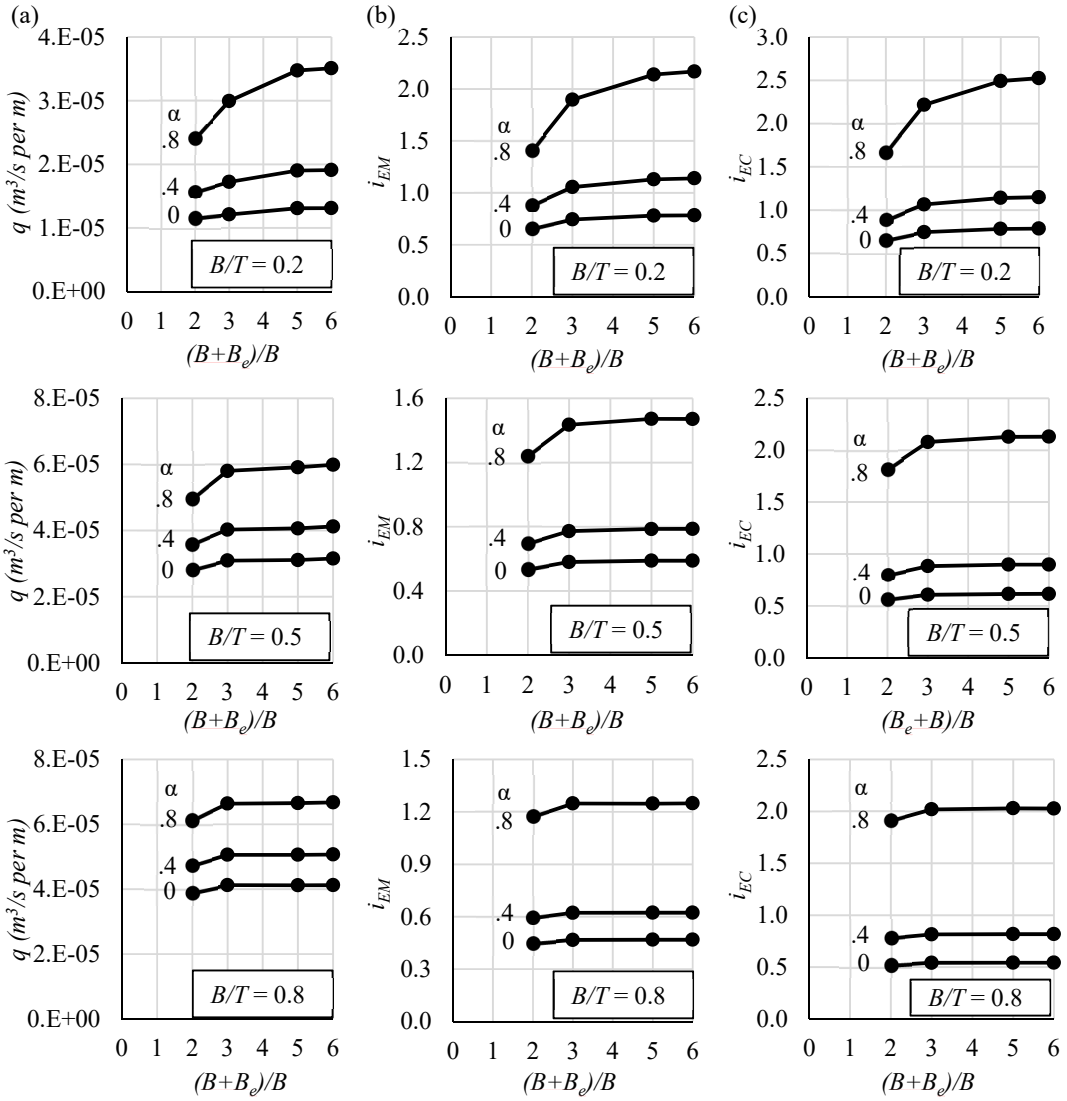

Fig. 6. Sensitivity analysis results for square cofferdams (a) flow rate; (b) exit gradient at mid-section (c) exit gradient at corner

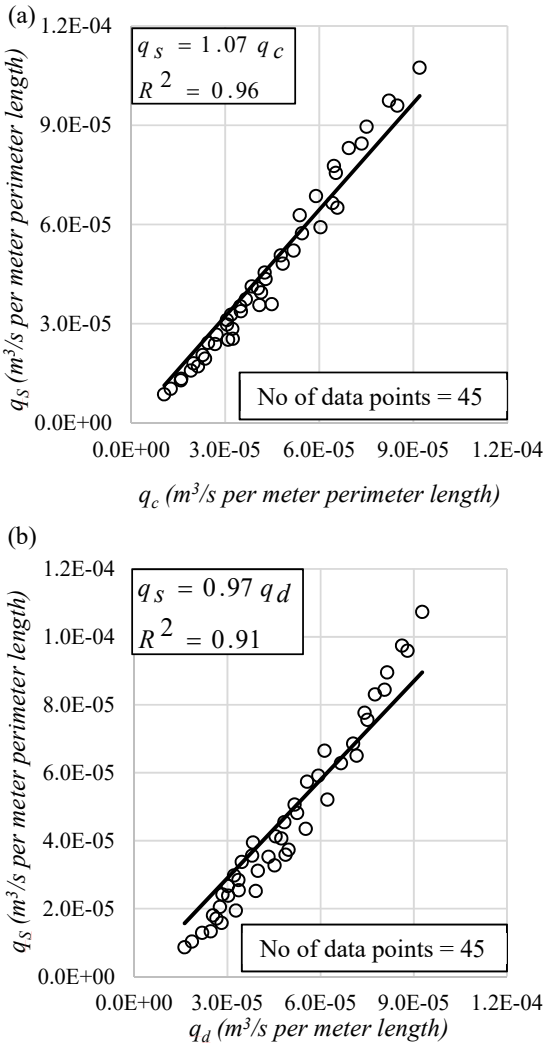

Fig. 7. Relationship between 2D flow rates to the 3D flow rate into square cofferdam; (a) axisymmetric flow (b) Cartesian flow

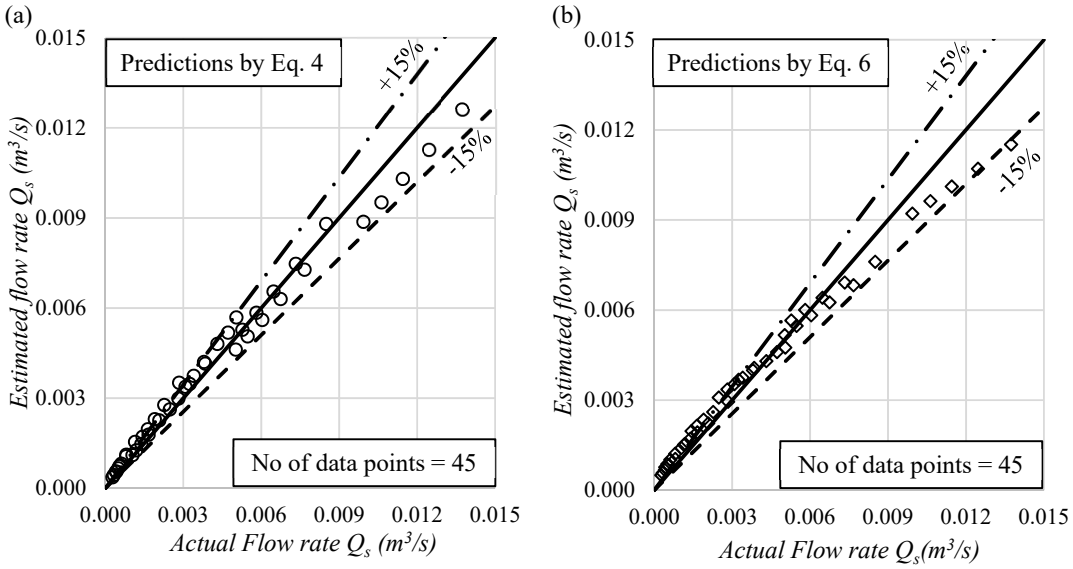

Fig. 8. Comparison of the flow rate predictions for square cofferdams using 2D flow patterns; (a) axisymmetric flow (b) Cartesian flow

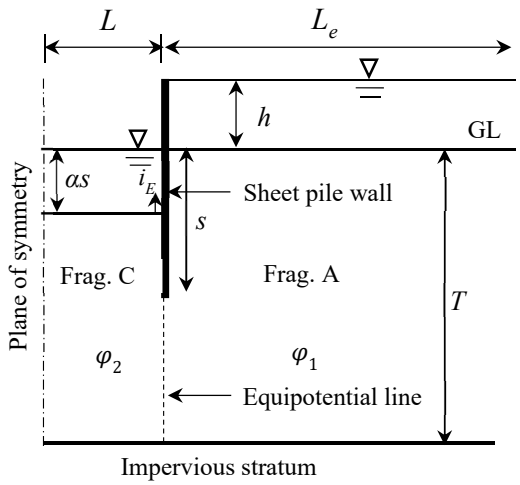

Fig. 9. Method of fragments (MoF) in double-walled cofferdam

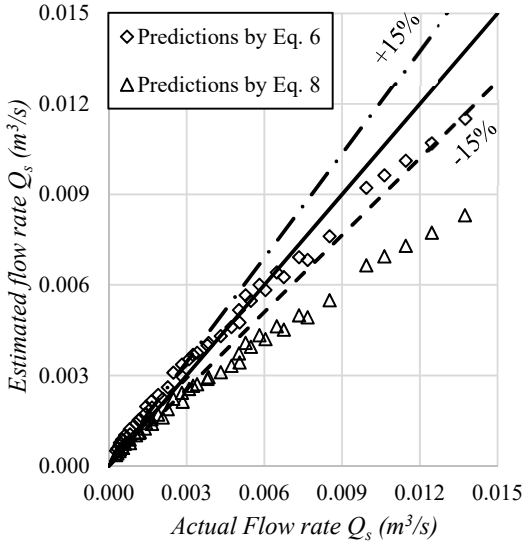

Fig. 10. Deviation of the flow rate predictions by Eq. 6 and Eq. 8 from the actual flow rate

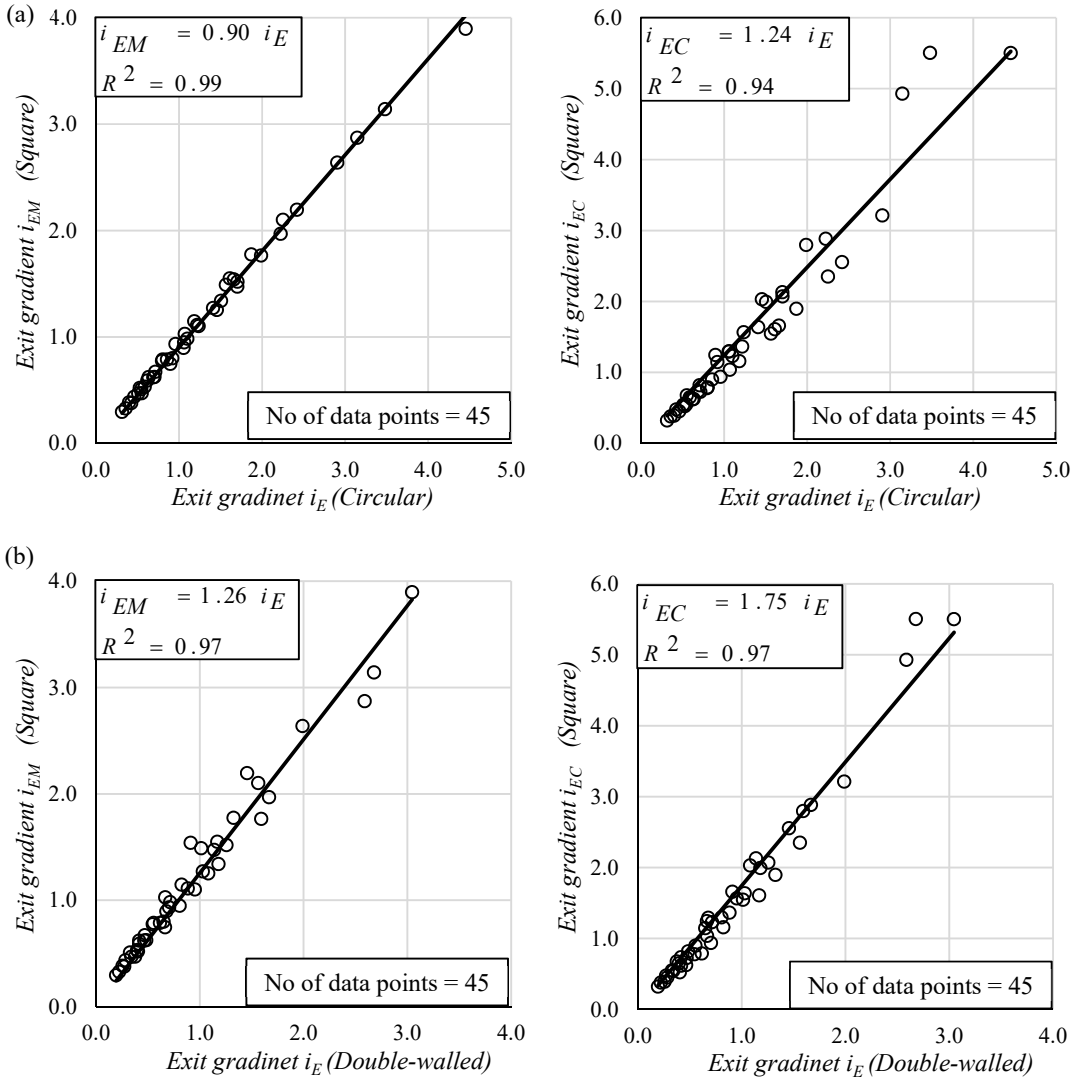

Fig. 11. Relationships between 2D exit gradient i_E values and the actual exit gradient values of square cofferdams i_{EM} and i_{EC} : (a) axisymmetric flow (b) Cartesian flow

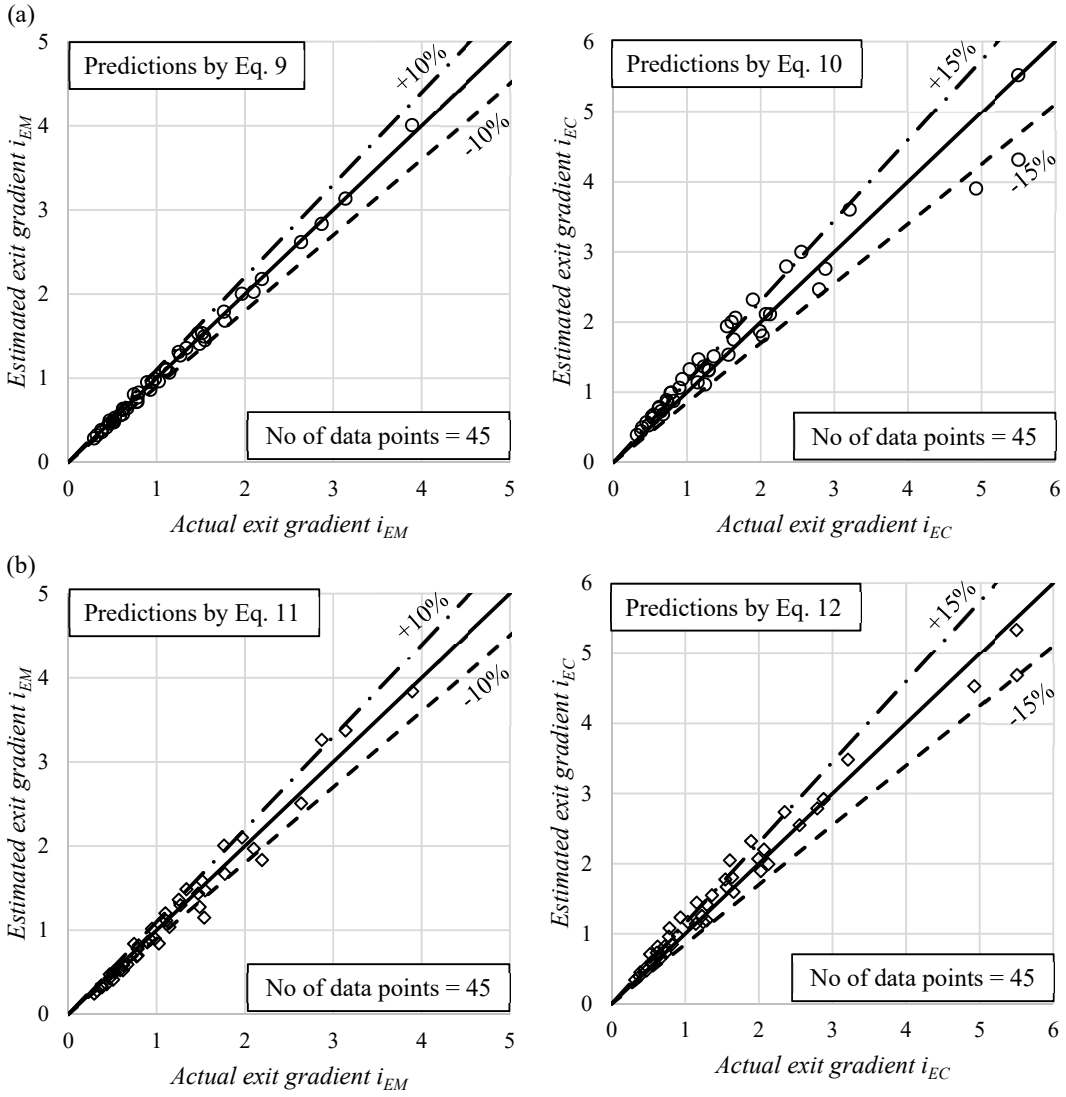

Fig. 12. Comparison of the exit gradient predictions using 2D flow patterns (a) axisymmetric flow (b) Cartesian flow

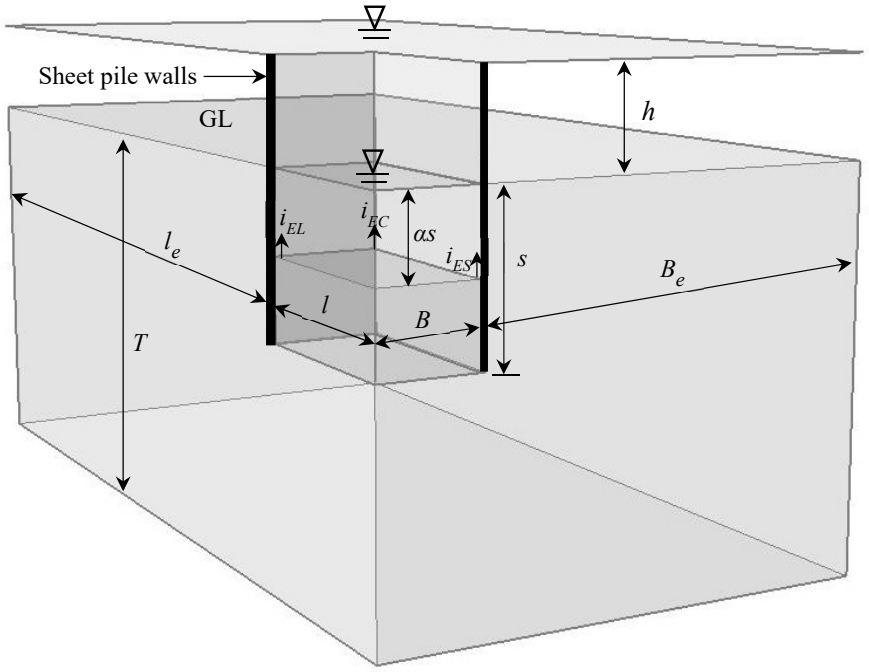

Fig. 13. Numerical model for rectangular cofferdam

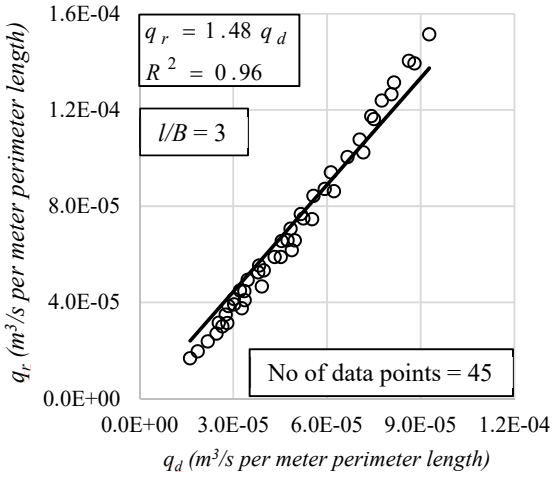

Fig. 14. Relationship between double-walled flow rate to the 3D flow rate into rectangular cofferdam

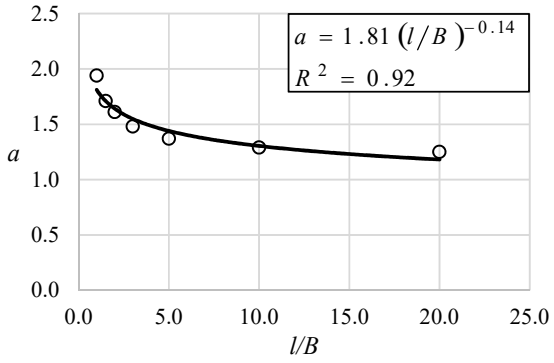

Fig. 15. Relationship of *a* value to the *l/B* ratio

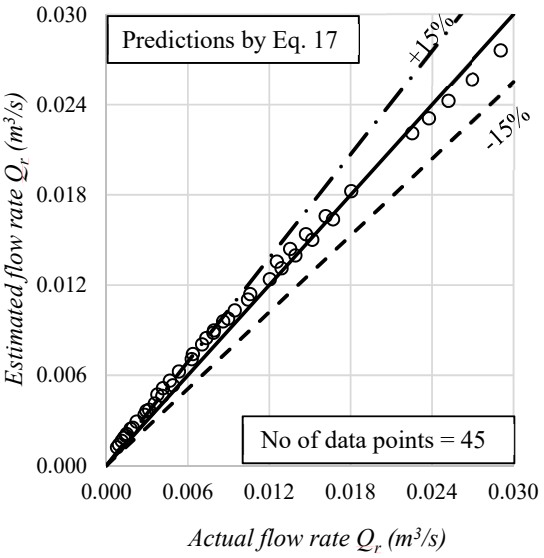

Fig. 16. Comparison of the flow rate predictions for rectangular cofferdam

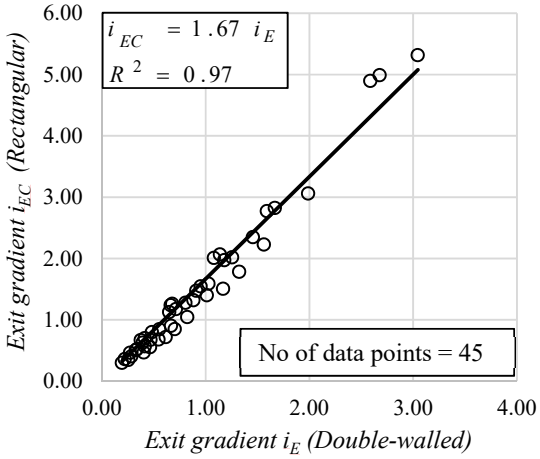

Fig. 17. Relationship between double-walled exit gradient to the actual exit gradient values of rectangular cofferdams with $l/B = 3$

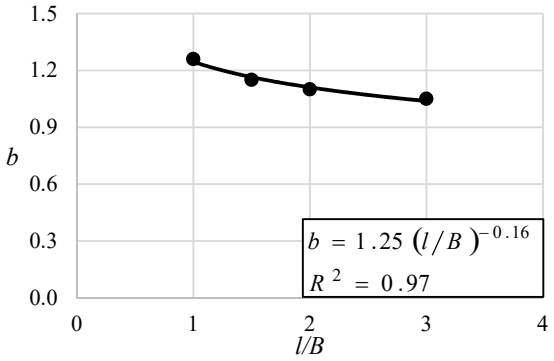

Fig. 18. Relationship of b value to the l/B ratio on i_{EL} estimation

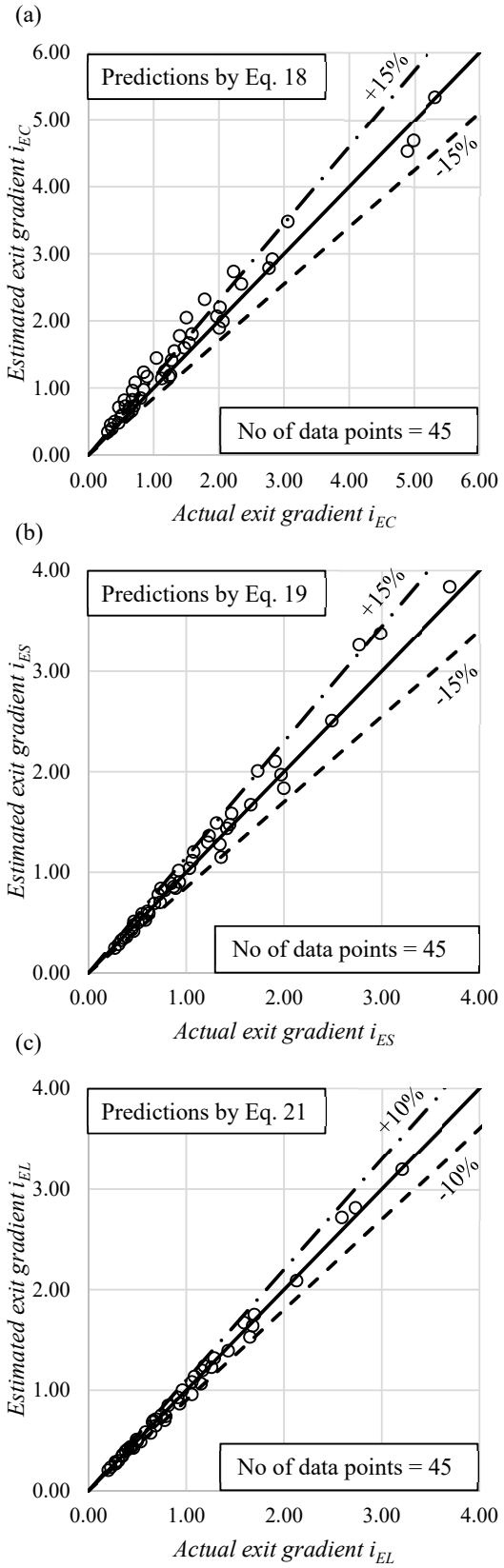

Fig. 19. Comparison of the exit gradient predictions for rectangular cofferdams

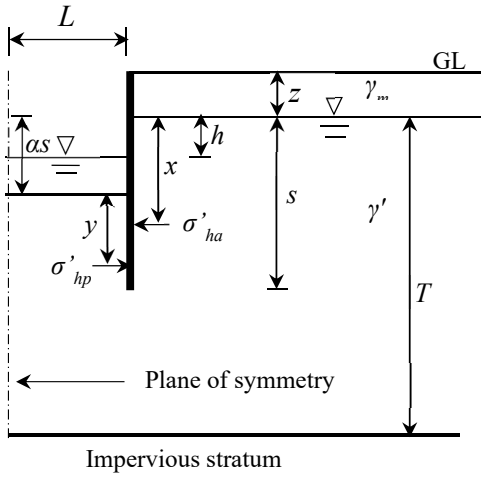

Fig. 20. Earth pressure when seepage presence for double-walled cofferdams